

AD-A075 133

NAVAL RESEARCH LAB WASHINGTON DC

F/G 20/5

METHODS OF EFFICIENCY ENHANCEMENT AND SCALING FOR THE GYROTRON --ETC(U)

SEP 79 K R CHU , M E READ , A K GANGULY

DOE-DE-AC01-79ET52053

UNCLASSIFIED

NRL-MR-4051

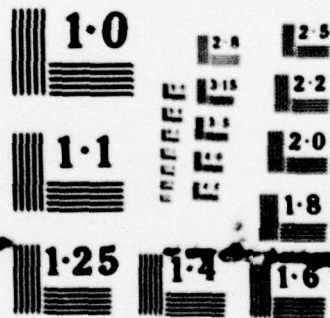
NL

1 OF 1  
AD-A075133



END  
DATE  
FILMED

11-79  
DDC



NATIONAL BUREAU OF STANDARDS  
MICROCOPY RESOLUTION TEST CHART

AD A075133

12

NRL Memorandum Report 4051

# Methods of Efficiency Enhancement and Scaling for the Gyrotron Oscillator

K. R. CHU AND M. E. READ

*Plasma Physics Division*

A. K. GANGULY

*Electronics Technology Division*

LEVEL II

September 20, 1979

DDC  
REF ID: A66116  
OCT 18 1979  
REGISTERED  
A



NAVAL RESEARCH LABORATORY  
Washington, D.C.

Approved for public release; distribution unlimited.

DDC FILE COPY

79 10 16 114



SECURITY CLASSIFICATION OF THIS PAGE (When Data Entered)

REPORT DOCUMENTATION PAGE		READ INSTRUCTIONS BEFORE COMPLETING FORM
1. REPORT NUMBER NRL Memorandum Report 4051	2. GOVT ACCESSION NO.	3. RECIPIENT'S CATALOG NUMBER <b>14</b> NRL-MR-4051
4. TITLE (and Subtitle) <b>6</b> METHODS OF EFFICIENCY ENHANCEMENT AND SCALING FOR THE GYROTRON OSCILLATOR		5. TYPE OF REPORT & PERIOD COVERED <b>7</b> Interim report on a continuing NRL problem
7. AUTHOR(s) <b>10</b> K. R. Chu, M. E. Read, and A. K. Ganguly		6. PERFORMING ORG. REPORT NUMBER
8. PERFORMING ORGANIZATION NAME AND ADDRESS Naval Research Laboratory Washington, D.C. 20375		9. CONTRACT OR GRANT NUMBER(s)
11. CONTROLLING OFFICE NAME AND ADDRESS Department of Energy Washington, D.C. 20585		10. PROGRAM ELEMENT PROJECT, TASK AREA & WORK UNIT NUMBERS NRL Problem R18-12 DOE- <del>XXXXXXXXXX</del> DE-AC01-79ET52053
14. MONITORING AGENCY NAME & ADDRESS (if different from Controlling Office) <b>11 21</b> <b>12 29</b>		12. REPORT DATE Sep <del>XXXXXX</del> 79
		13. NUMBER OF PAGES 28
		15. SECURITY CLASS. (of this report) UNCLASSIFIED
		15a. DECLASSIFICATION/DOWNGRADING SCHEDULE
16. DISTRIBUTION STATEMENT (of this Report) Approved for public release; distribution unlimited		
17. DISTRIBUTION STATEMENT (of the abstract entered in Block 20, if different from Report)		
18. SUPPLEMENTARY NOTES		
19. KEY WORDS (Continue on reverse side if necessary and identify by block number) Gyrotron Oscillator Efficiency Enhancement and Scaling ABSTRACT		
20. ABSTRACT (Continue on reverse side if necessary and identify by block number) It is shown that a gyrotron oscillator operating in a slightly tapered magnetic field can attain an efficiency of 78%, approximately 1.7 times higher than that obtainable in a constant magnetic field. Extensive numerical data have been tabulated and a convenient parameter is introduced to generate numerical efficiency scaling relations through which optimum operating conditions are clearly exhibited. Conditions for reaching the high efficiency operating regime have also been studied and are numerically illustrated.		

DD FORM 1473

EDITION OF 1 NOV 65 IS OBSOLETE  
S/N 0102-014-6601

SECURITY CLASSIFICATION OF THIS PAGE (When Data Entered)

251 950

mt



## CONTENTS

I. INTRODUCTION .....	1
II. MODEL, ASSUMPTIONS, AND BASIC EQUATIONS .....	4
III. RESULTS .....	8
IV. ACCESSIBILITY OF THE HIGH EFFICIENCY REGIME .....	11
V. DISCUSSION .....	13
REFERENCES .....	14

<b>Accession For</b>	
NTIS GRA&I	<input checked="checked" type="checkbox"/>
DDC TAB	<input type="checkbox"/>
Unannounced	<input type="checkbox"/>
Justification	
By _____	
Distribution/ _____	
<b>Availability Codes</b>	
Dist	Avail and/or special
A	

## **Methods of Efficiency Enhancement and Scaling for the Gyrotron Oscillator**

### **I. INTRODUCTION**

The gyrotron is a microwave device based on the cyclotron maser interaction between an electromagnetic wave and an electron beam in which the individual electrons move along helical trajectories in the presence of an applied magnetic field. In recent years, it has emerged as a new and by far the most powerful source of millimeter and submillimeter radiation. Potential applications of the gyrotron includes radar, communication, and plasma heating of controlled nuclear fusion devices. Most of the work on gyrotrons, both theoretical and experimental, has been carried out for two basic configurations: (i) the single cavity configuration, and (ii) the waveguide configuration. In the first configuration (the gyrotron oscillator), the electron beam sustains a constant amplitude normal mode oscillation in an open end cavity. In the second configuration (the gyrotron travelling wave amplifier), the electron beam amplifies the normal mode of a fast waveguide structure. A detailed analysis of the cyclotron maser mechanism<sup>1</sup> as well as review articles<sup>2,3</sup> on the gyrotron development can be found in recent literature.

The present work proposes a method for enhancing the efficiency of gyrotron oscillators and studies the scaling of efficiency with respect to the operating parameters.

Our primary motivation for achieving a high efficiency gyrotron is connected with its application in controlled fusion research. To reach the fusion ignition temperature, a great



amount of energy (many megajoules) has to be injected for plasma heating. Furthermore, this should be done with the maximum efficiency in order to alleviate the energy breakeven condition. A highly efficient gyrotron has been recognized as one of the most promising sources to meet these requirements. Many methods for efficiency enhancement have so far been considered. These methods are largely variations of two general approaches. The first approach, emphasized by Soviet workers,<sup>4-11</sup> involves the contouring of the wave electric field profile. The second approach, employed by Sprangle and Smith<sup>12</sup> and also in the present paper, involves the contouring of the applied *dc* magnetic field. For a brief review of the previous results, two commonly used definitions of efficiency need to be distinguished. The overall efficiency ( $\eta$ ) is defined as the average electron energy loss divided by its total initial energy and the transverse efficiency ( $\eta_t$ ) is the same quantity divided by the initial transverse energy. Thus,  $\eta = 0.8\eta_t$  if  $v_\perp/v_\parallel = 2$ , and  $\eta = 0.7\eta_t$  if  $v_\perp/v_\parallel = 1.5$ . For a sinusoidal wave electric field profile, the maximum achievable efficiency ( $\eta$ ) is approximately<sup>13</sup> 42% for  $v_\perp/v_\parallel = 2$  and 35% for  $v_\perp/v_\parallel = 1.5$ . Using a Gaussian wave electric field profile and  $v_\perp/v_\parallel = 1.5$ , Nasinovich et al.<sup>5,10</sup> have shown that  $\eta_t$  can reach 79% (or  $\eta = 55\%$ ). Using a more complicated (axially asymmetric) wave electric field profile, Kolosov and Kurayev<sup>7</sup> have calculated a maximum transverse efficiency of 88%. The above figures all refer to the fundamental cyclotron harmonic. However, it has been shown in Refs. 7 and 10 that the maximum efficiency at the second cyclotron harmonic differs only slightly from that of the fundamental cyclotron harmonic. In practice, the wave electric field contouring can be achieved by contouring the cross-section of the cavity<sup>11</sup>, as is done by Kisel et al.<sup>9</sup> In the case of applied magnetic field contouring, Sprangle and Smith<sup>12</sup> proposed a method which employs a two-stage magnetic field. Except for a short transition region, the magnetic field is held constant in each stage. In the first stage, the magnetic field is below that required for strong resonant interaction, hence only electron bunching takes place. In the second stage, the magnetic field is raised to the value for



strong interaction, thus allowing the bunched electrons to lose a substantial amount of energy. They have calculated a maximum transverse efficiency of 75% (or  $\eta = 60$  for  $v_{\perp}/v_{\parallel} = 2$ ). Because of the presence of a bunching stage, a relatively longer cavity is required in their scheme. This may become a rather strong limiting factor in high power operations.

In the present study a linearly tapered magnetic field is employed for the purpose of efficiency enhancement. The magnetic field increases uniformly over the length of the cavity with approximately a 10% variation from end to end. For  $v_{\perp}/v_{\parallel} = 1.5, 2$ , and  $2.5$ , we have calculated a maximum efficiency of 56%, 67%, and 78%, respectively (corresponding to  $\eta_{\perp} = 80\%$ , 84%, and 90%, respectively). Compared with the other methods discussed above, this method promises a very high efficiency with the simplest structure.

As shown in a recent linear analysis,<sup>14</sup> the nature of the cyclotron maser interaction in a gyrotron is much more complicated than that in a gyrotron travelling wave amplifier mainly because the electromagnetic wave in a cavity consists of both a forward and a backward component as compared with a single forward component in the waveguide. As a result, nonlinear analysis of the gyrotron oscillator, mainly the calculation of its efficiency, becomes difficult to treat analytically. Thus far, practically all the nonlinear analyses of gyrotron oscillators (including the present one) have been based on numerical computation. In comparison, the nonlinear analyses<sup>15-17</sup> of gyrotron travelling wave amplifiers have been more analytical in nature. While the numerical approach allows one to employ more exact physical models, it often fails to show the general properties of the system examined. This limitation has made it difficult to identify the optimum modes and parameters of operation from a great number of possibilities. Thus a second objective of the present paper is to seek from the extensive numerical data obtained a simple efficiency scaling relation which clearly shows the optimum operating conditions. We

found that there exists a common parameter  $N_c$ , i.e. the total number of cyclotron orbits executed by an electron in traversing the cavity, which connects the seemingly random data into smooth curves. Indeed, as the final result will indicate,  $N_c$  appears to be a convenient parameter for generating the common operating characteristics for gyrotron oscillators operating at different modes.

The paper is organized as follows. In Sec. II, we present the model, assumptions, and the basic gyrotron equations. In Sec. III, the main results are obtained and a design example is given on the basis of the optimized data. In Sec. IV, we study the accessibility of the high efficiency regime, a problem of considerable practical importance but not yet addressed theoretically. Sec. V contains further discussions.

## II. MODEL, ASSUMPTIONS, AND BASIC EQUATIONS

Figures 1(a) and (b) shown the single cavity gyrotron oscillator model under study. An annular electron beam is injected into an open-end cavity from the left hand side and propagates to the right under the guidance of an applied magnetic field  $B_0$  [Fig. 1(a)]. The electrons, moving along helical trajectories, have a substantial part of their kinetic energy in the form of transverse motion. Inside the cavity, the electron beam gives up a portion of its energy through interaction with the EM fields. If the average power lost by the beam equals the wave power diffracted out of the cavity, a steady state is then established. A main objective of our calculation is to maximize the beam energy loss at the steady state. The electron beam is typically generated from a magnetron type electron gun. Both theory<sup>1a</sup> and experiment have shown that a beam so generated has the desirable properties for gyrotron applications, namely, it is thin and cold. Thus, in our model we assume that the beam electrons are monoenergetic with their guiding centers located on the same surface of constant radius ( $r = r_0$ ). Figure 1(b)



shows the cross-sectional view of the model. We assume further that the beam is sufficiently tenuous that its space charge field can be neglected and that it will not modify the normal mode EM field structure of the cavity. This is a good assumption for beam powers below a few hundred kW. Since the cyclotron maser interaction takes place between the electron beam and the TE mode (rather than the TM mode) and axially symmetric TE modes (i.e. modes without azimuthal variations) have the smallest wall loss, we will limit our consideration to the  $TE_{0nl}$  modes, where  $n$  and  $l$  are, respectively, the radial and axial eigenmode numbers. Under these assumptions, the electron dynamics are governed by the following equation of motion,

$$\frac{d}{dt} \gamma m \mathbf{v} = -e(\mathbf{E} + \mathbf{v} \times \mathbf{B}) , \quad (1)$$

where  $\gamma = (1 - v^2/c^2)^{-1/2}$ ,  $\mathbf{E} = E_\theta \mathbf{e}_\theta$ ,  $\mathbf{B} = \mathbf{B}_0 + B_r \mathbf{e}_r + B_z \mathbf{e}_z$ ,  $\mathbf{B}_0$  is the applied magnetic field (to be specified later), and  $E_\theta$ ,  $B_r$ ,  $B_z$  are the  $TE_{0nl}$  wave fields given by,

$$E_\theta = E_{\theta 0} J_1(k_n r) \sin k_z z \cos \omega t , \quad (2)$$

$$B_r = (k_z/\omega) E_{\theta 0} J_1(k_n r) \cos k_z z \sin \omega t , \quad (3)$$

$$B_z = -(k_n/\omega) E_{\theta 0} J_0(k_n r) \sin k_z z \sin \omega t , \quad (4)$$

where  $k_z = \pi l/L$ ,  $k_n = x_n/r_a$ ,  $x_n$  is the  $n$ th nonvanishing root of  $J_1(x) = 0$ ,  $\omega = (k_z^2 + k_n^2)^{1/2} c$  is the wave frequency, and  $r_a$  is the inner radius of the cavity.

The total wave energy stored in the cavity ( $W_f$ ) can be written,

$$W_f = 0.25 \pi \epsilon_0 E_{\theta 0}^2 J_0^2(x_n) r_a^2 L ,$$

where  $\epsilon_0 = (36\pi)^{-1} 10^{-9}$  farad/m is the vacuum dielectric constant and  $J_0^2(x_n) \approx 0.16, 0.09, 0.0625$  for  $n = 1, 2, 3$ . If we assume that the quality factor  $Q$  of the cavity is entirely due to diffraction loss (i.e. neglecting wall loss), we obtain the wave power ( $P_w$ ) emitted from the cavity

$$\begin{aligned} P_w &= \omega W_f / Q \\ &= 0.25 \pi \epsilon_0 \omega E_{\theta 0}^2 J_0^2(x_n) r_a^2 L / Q \end{aligned} \quad (5)$$



Thus, the beam power ( $P_b$ ), required to sustain a steady state oscillation in the cavity is

$$P_b = P_w/\eta$$

$$= 0.25\pi\epsilon_0\omega E_{00}^2 J_0^2(x_n) r_w^2 L/\eta Q \quad (6)$$

where  $\eta$  is the efficiency to be evaluated from Eq. (1).

It is convenient to introduce a normalization scheme by which the cavity radius  $r_w$  is scaled out of the equations. This can be achieved through the following procedures (normalized notations are denoted by a bar):

- (i) length normalized to  $r_w$  ( $\bar{r} = r/r_w$ );
- (ii) frequency normalized to  $c/r_w$  ( $\bar{\omega} = \omega r_w/c$ );
- (iii) velocity normalized to  $c$  ( $\bar{v} = v/c$ ); and
- (iv) electric and magnetic field normalized to  $mc^2/er_w$  and  $mc/er_w$ , respectively ( $\bar{E}_\theta = E_\theta er_w/mc^2$ ,  $\bar{B}_\theta = B_\theta er_w/mc$ ).

Other quantities such as  $k_z$  and  $t$  are to be normalized consistently with the preceding procedures ( $\bar{k}_z = k_z r_w$ ,  $\bar{t} = tc/r_w$ ). However, naturally dimensionless quantities such as  $\gamma$  and  $\eta$  will remain unchanged. Results obtained under the normalized representation are thus applicable to cavities of arbitrary radius.

We may now rewrite Eqs. (1)-(6) as

$$\frac{d}{dt} \gamma m \bar{v} = -(\bar{E} + \bar{v} \times \bar{B}) \quad (7)$$

$$E_\theta = \bar{E}_{\theta 0} J_1(x_n \bar{r}) \sin \bar{k}_z \bar{z} \cos \bar{\omega} \bar{t}, \quad (8)$$

$$\bar{B}_r = (\bar{k}_z/\bar{\omega}) \bar{E}_{\theta 0} J_1(x_n \bar{r}) \cos \bar{k}_z \bar{z} \sin \bar{\omega} \bar{t}, \quad (9)$$

$$\bar{B}_z = -(x_n/\bar{\omega}) \bar{E}_{\theta 0} J_0(x_n \bar{r}) \sin \bar{k}_z \bar{z} \sin \bar{\omega} \bar{t}, \quad (10)$$

$$QP_w = 548 \bar{\omega} \bar{E}_{\theta 0}^2 J_0^2(x_n) \bar{L} \text{ MW}, \quad (11)$$

and

$$QP_s = 548 \bar{\omega} \bar{E}_{s0}^2 J_0^2(x_s) \bar{L} / \eta \text{ MW} . \quad (12)$$

To obtain the efficiency from this set of equations, we solve Eq. (7) numerically for the energy loss (or gain) by a single electron in traversing the cavity. The efficiency is then evaluated by averaging over an ensemble of electrons uniformly distributed in their initial gyration phase angle  $\phi$  (Fig. 1b). In solving Eq. (7), the following initial conditions and parameters need to be specified: The initial electron energy ( $\gamma_0$ ) and velocity ratio ( $\alpha \equiv v_{\perp 0}/v_{\parallel 0}$ ), the initial electron guiding center position ( $\bar{r}_0$ ), the cavity dimension ( $\bar{L}$ ), the mode numbers ( $n$  and  $h$ ), the wave field strength ( $\bar{E}_{s0}$ ), and the applied magnetic field profile ( $\bar{\mathbf{B}}_0$ ) defined below,

$$\bar{\mathbf{B}}_0(\bar{r}, \bar{z}) = \bar{B}_{0r} \mathbf{e}_r + \bar{B}_{0z} \mathbf{e}_z \quad (13)$$

where

$$\bar{B}_{0r}(\bar{r}) = -\frac{1}{2} \Delta \bar{B} \bar{r} / \bar{L} , \quad (14)$$

and

$$\bar{B}_{0z}(\bar{z}) = \bar{B}_1 + \Delta \bar{B} \bar{z} / \bar{L} . \quad (15)$$

Figure 2 shows the axial magnetic field ( $\bar{B}_{0z}$ ) profile inside the cavity. The variation of  $\bar{B}_{0z}$  is typically in the neighborhood of 10%, hence  $\bar{\mathbf{B}}_0$  points predominantly in the  $z$ -direction. For comparison, we will also calculate the efficiency for a constant applied magnetic field, in which case  $\bar{\mathbf{B}}_0$  is simply

$$\bar{\mathbf{B}}_0 = \bar{B}_0 \mathbf{e}_z \quad (16)$$

where  $\bar{B}_0$  is a constant.

The beam guiding center position for maximum coupling with the wave has been calculated in Ref. 14. Here we will limit our consideration to the case of fundamental cyclotron harmonic interaction and  $\bar{r}_0$  for maximum beam-wave coupling is given by,<sup>14</sup>



$$\bar{r}_0 = 1.8/x_n, \quad (16)$$

where  $x_n = 3.8, 7.0$  and  $10.2$  for  $n = 1, 2, 3$ , respectively. To reduce the number of free parameters, we fix the electron energy at 70 keV. This is a voltage capable of generating a sufficiently high power electron beam for most applications presently conceived, including plasma heating of controlled fusion devices. The axial eigenmode number will be fixed at the lowest value ( $l = 1$ ) because it gives the highest cavity  $Q$  and hence the lowest threshold beam power compared with the  $l \neq 1$  modes. Thus the unwanted high  $l$  modes will not be excited if one operates near the threshold of the  $l = 1$  mode. The remaining parameters,  $\alpha$ ,  $\bar{L}$ ,  $n$ ,  $\bar{E}_{\theta 0}$ ,  $\bar{B}_0$ ,  $\bar{B}_1$ , and  $\Delta\bar{B}$  etc., will be varied.

### III. RESULTS

A typical data point is obtained as follows. We first specify  $\alpha$ ,  $\bar{L}$ , and  $n$ . In the case of tapered magnetic field, the efficiency  $\eta$  is then evaluated as a function of  $\bar{E}_{\theta 0}$ ,  $\bar{B}_1$ , and  $\Delta\bar{B}$ . The point where  $\eta(\bar{E}_{\theta 0}, \bar{B}_1, \Delta\bar{B})$  peaks will be taken as a data point and referred to as the optimum efficiency,  $\eta^{op}$ . In the case of constant magnetic field,  $\eta$  is evaluated as a function of  $E_{\theta 0}$  and  $\bar{B}_0$ , and similarly the peak of  $\eta(\bar{E}_{\theta 0}, \bar{B}_0)$  becomes a data point.

As a check of the numerical accuracy, we monitor a constant of motion, the canonical angular momentum  $\bar{P}_\theta (\equiv \gamma \bar{r} v_\theta - \bar{r} \bar{A}_\theta)$ , where  $\bar{A}_\theta$  is the vector potential of the EM fields). In all the numerical runs,  $\bar{P}_\theta$  is found to fluctuate not more than  $10^{-5}$ , an indication of good numerical accuracy.

Tables I, III, and V list the optimum efficiency data obtained for the tapered magnetic field profile. Each table applies to a fixed value of  $\alpha (\equiv v_{\perp 0}/v_{\parallel 0})$ , while entries in the same table are for various mode numbers ( $n$ ) and cavity length ( $\bar{L}$ ). For comparison, Tables II, IV, and VI list the corresponding optimum efficiency data obtained for a constant magnetic field



profile. In Tables I through VI,  $QP_b^{\text{op}}$  is the product of the quality factor  $Q$  and the beam power at optimum efficiency operation. Similarly  $QP_b^{\text{th}}$  is  $Q$  times the threshold beam power required to start the oscillation under conditions optimized for efficiency. The significance of  $P_b^{\text{th}}$  will be discussed further in Sec. IV.

In all the data presented, we have kept track of a common parameter  $N_c$ , the total number of cyclotron orbit executed by a single electron in traversing the cavity. To illustrate the efficiency scaling with respect to  $N_c$  and the efficiency enhancement due to magnetic field tapering, we have plotted  $\eta^{\text{op}}$  against  $N_c$  in Fig. 3a, b, and c. In these and all the subsequent figures, solid curves refer to the tapered magnetic field and dashed curves refer to the constant magnetic field. The lowest curves in Figs. 3a, b, and c give  $\Delta\bar{B}/\bar{B}_1$ , a measure of the magnetic field tapering (see Fig. 2). The numbered dots refer to the data No. in Tables I through VI. Figure 4 shows typical plots of efficiency versus the axial distance inside the cavity. It is seen that in both the tapered and constant magnetic field cases, strong interaction (as witnessed by the rapid rise of efficiency) takes place after an initial bunching stage. However, in a tapered magnetic field, the region of strong interaction stretches farther at both ends, resulting in higher efficiency.

On the basis of the data presented here, we may summarize the principal results as follows:

(1) With magnetic field tapering, one can enhance the peak efficiency by a factor of 1.6 to 1.7 over what is obtainable in a constant magnetic field and the required amount of tapering ( $\Delta\bar{B}/\bar{B}_1$ ) is only a few percent (Fig. 3). The higher the velocity ratio  $\alpha$ , the higher the maximum achievable efficiency. The peak efficiencies for  $\alpha = 1.5, 2.0$ , and  $2.5$  as shown in Fig. 3 are, respectively, 34.9%, 41.2%, and 44.4% for the constant magnetic field and 55.7%, 67.1%,

and 77.8% for the tapered magnetic field. Currently available electron beams have a maximum  $\alpha$  value of  $\sim 2$ , hence a 67% efficiency can be achieved (in a tapered magnetic field) with the present technology. For the purpose of further efficiency enhancement, it is desirable to improve the electron gun design so that beams with higher  $\alpha$  can be obtained.

(2)  $N_c$  is shown to be a convenient scaling parameter for the efficiency for both the constant and tapered magnetic field cases (Fig. 3). We observe in Fig. 3 that for a fixed  $\alpha$ , the efficiency data calculated for various modes ( $n$ ) and cavity dimensions ( $\bar{L}$ ) form a single curve when plotted against  $N_c$ . In other words, the efficiency is only a function of  $N_c$  regardless of the mode of operation and the dimension of the cavity. Thus, for modes and cavity dimensions not calculated here, one can predict its efficiency by simply calculating the value of  $N_c$  and interpolating from the data presented. Similarly, through this method of scaling, efficiency optimization for any given mode of operation becomes a simple task of specifying the cavity length such that  $N_c$  has the value corresponding to the peak efficiency in Fig. 3. In general, the efficiency peaks at  $20 < N_c < 30$ , which can be used as a crude guide for the design of gyrotron oscillators. It will be shown in Sec. IV that  $N_c$  also serves as a useful parameter for determining the accessibility of the high efficiency regime.

(3) The wave electric field  $E_{w0}$  at optimum efficiency operation is stronger for the tapered magnetic field case than for the constant magnetic field case because more beam energy has to be extracted in the former case to reach the higher efficiency (cf. Table I through VI). As a result, one gains the additional advantage of achieving higher wave power as well as higher efficiency by tapering the magnetic field. Near the peak efficiency, for example,  $QP_s$  for the tapered magnetic field is higher than that for the constant magnetic field by a factor  $> 2$ .



We conclude this section with a specific design example based data no. 14 in Table III. To convert the normalized data quantities into physical design parameters, one needs to specify the desired wave frequency ( $f$ ) and the quality factor  $Q$ . In the example, we shall let  $f = 35$  GHz and  $Q = 500$ . The wall radius ( $r_w$ ) is given by

$$r_w = 4.775 \bar{\omega} / f \text{ cm},$$

where  $f$  is in GHz. From Table III, we obtain  $\bar{\omega} = 3.85$ . Thus,  $r_w = 0.526$  cm. In terms of  $r_w$ , the cavity length ( $L$ ), the beam guiding center position ( $r_0$ ), the magnetic field profile ( $B_1$  and  $\Delta B$ ), and the wave electric field amplitude ( $E_{\theta 0}$ ) can all be specified through the following formulae:

$$L = \bar{L} r_w \text{ cm},$$

$$r_0 = \bar{r}_0 r_w \text{ cm},$$

$$\begin{pmatrix} B_1 \\ \Delta B \end{pmatrix} = 1.707 r_w^{-1} \begin{pmatrix} \bar{B}_1 \\ \bar{\Delta B} \end{pmatrix} \text{ kG},$$

and

$$E_{\theta 0} = 512.1 r_w^{-1} \bar{E}_{\theta 0} \text{ kV/cm},$$

where  $r_w$  is in unit of cm. Finally, dividing  $QP_b^{th}$  and  $QP_b^{op}$  by  $Q$  gives, respectively,  $P_b^{th}$  and  $P_b^{op}$ . Table VII lists the parameters of the 35 GHz gyrotron oscillator design example.

#### IV. ACCESSIBILITY OF THE HIGH EFFICIENCY REGIME

A comparison between the small signal theory of Ref. 14 and the present large signal theory shows that the optimum conditions for small and large signal interactions are close but not identical. Furthermore, the difference becomes more and more pronounced as  $N_c$  increases. As an example, we consider the following three cases involving a constant magnetic field (cf. data no. 18, 19, and 20 in Table IV): (i)  $TE_{011}$  mode,  $\bar{L} = 5$ ,  $N_c = 13.4$ , (ii)  $TE_{011}$  mode,  $\bar{L} = 8$ ,  $N_c = 21.5$ , and (iii)  $TE_{021}$  mode,  $\bar{L} = 5$ ,  $N_c = 24.7$ . As shown in Table IV, optimum efficiency operation requires a magnetic field ( $\bar{B}_0$ ) of 4.126, 4.142, and 7.607 for cases (i), (ii),



and (iii), respectively, while the small signal theory<sup>14</sup> predicts that strongest interaction occurs at  $\bar{B}_0 = 4.242, 4.276$ , and  $7.855$  for the same cases. Thus, optimum magnetic field in the small signal regime is higher than that in the larger signal regime by 2.8%, 3.2%, and 3.3%, respectively, for the three cases. This raises a question concerning the accessibility of the high efficiency (large signal) regime. Consider, for example, an experiment in which parameters are optimized for high efficiency operation. To reach the large signal operating regime, one has to first start from the small signal regime. But since the experimental parameters are not optimum for the transient small signal regime, the beam power required to start the small signal oscillation may be higher than the beam power ( $P_h^{op}$ ) required for the large signal operation. As a result, the oscillation can not be started with the designed beam power  $P_h^{op}$ . This point is quantitatively illustrated in Fig. 5 (a), (b), and (c), where  $QP_h$  and  $\eta$  for the three cases just considered are plotted against  $QP_u$ , a quantity proportional to the field energy in the cavity. In addition, the three corresponding cases (data No. 13, 14, and 15 in Table III) involving tapered magnetic field are also plotted. Note that the magnetic fields used in obtaining Fig. 5 are those shown in Tables III and IV which are optimized for high efficiency rather than for small signal interaction.  $P_h$  in the limit of small cavity field ( $P_u \rightarrow 0$ ) is defined as  $P_h^{th}$ , and  $P_h$  corresponding to the peak of  $\eta$  is referred to as  $P_h^{op}$ . For case (i) where  $N_c = 13.5$ , the difference between the optimum conditions for the small and large signal regimes is insignificant so that  $P_h^{th}$  is well below  $P_h^{op}$  and the large signal regime is easily accessible. For case (ii) where  $N_c = 21.5$ , the difference becomes more pronounced such that  $P_h^{th}$  is comparable to  $P_h^{op}$ . Still, the oscillation can be started with a beam power slightly greater than  $P_h^{op}$ . For case (iii), however, the difference becomes so great that  $P_h^{th}$  is well above  $P_h^{op}$ . In which case, one of the following procedures would have to be taken to reach the high efficiency regime. (1) One initially operates with a beam power greater than  $P_h^{th}$  to build up the cavity field and later lower it to  $P_h^{op}$  to

achieve high efficiency; (2) one initially operates in a higher magnetic field for which  $P_h^{th}$  is below  $P_h^{op}$  and slowly lowers it to the designed value after the oscillation has started; and (3) one builds up the cavity field with externally injected wave to the point where it can be further pumped up with  $P_h^{op}$  to reach the high efficiency regime. It is interesting to note that Kisel et al.<sup>9</sup> have used procedure (2) to reach their high efficiency operating regime. The present analysis provides a theoretical interpretation of their procedure. We note also that in more severe cases, the beam actually absorbs the field energy in the small signal regime when conditions are optimized for high efficiency. Such cases are indicated by  $P_h^{th} = \infty$  in Tables I through VI.

## V. DISCUSSION

So far we have neglected the Ohmic power loss on the cavity wall. The results could be easily modified to incorporate the effect of Ohmic loss. In the presence of a resistive wall, a fraction of the extracted beam power will be dissipated in the wall as heat loss, the remaining fraction,  $F$ , comes out as wave power, where

$$F = Q_{ohm} / (Q_{ohm} + Q_d) .$$

and  $Q_{ohm}$  and  $Q_d$  are, respectively, the Ohmic and diffraction  $Q$  of the cavity as commonly defined. Thus, all the results remain valid provided that  $Q$  is now defined as  $Q = Q_{ohm} Q_d / (Q_{ohm} + Q_d)$  and that the calculated values of  $P_e$  and  $\eta$  are multiplied by the factor  $F$ .

In our calculations, we have always positioned the electron beam on the peak of the electric field. This has allowed us to obtain the maximum efficiency with the minimum beam power. For some applications, however, higher wave power is desired. This can be achieved without sacrifice in efficiency by positioning the beam away from the peak of the electric field. In such a case, the optimum wave electric field as shown in Tables I through VI refers to the



local field exerted on the electrons, and consequently the peak field is higher than that indicated in the Table, implying higher wave power and proportionally higher beam power under optimum operating conditions. For example, if the local electric field is half of the peak electric field, both the beam power and the wave power will be four times higher.

Here we have shown that a simple linearly tapered magnetic field (see Fig. 2) results in dramatic enhancement in efficiency. Although no calculations have been made for a more complicated magnetic field profile, it appears likely that variations from the linear profile may result in further efficiency enhancement. It is also expected that the ultimate efficiency limit may very well be achieved by a combination of magnetic field and wave electric field contouring. All these possibilities point out that further research in this area is warranted and will almost certainly lead to even more efficient gyrotrons.

The authors would like to thank Dr. P. Sprangle, Dr. V. L. Granatstein, and Dr. R. Smith for many stimulating discussions. This work was supported by U.S. Department of Energy, No. EX-77-A-34-1015.

#### REFERENCES

1. K. R. Chu and J. L. Hirshfield, "Comparative study of the axial and azimuthal bunching mechanisms in electromagnetic cyclotron instabilities," *Phys. Fluids*, vol. 21, pp. 461-466, 1978.
2. V. A. Flyagin, A. V. Gaponov, M. I. Petelin, and V. R. Yulpatov, "The gyrotron," *IEEE Trans. Microwave Theory Tech.*, vol. MTT-25, pp. 514-521, 1977.

3. J. L. Hirshfield and V. L. Granatstein, "The electron cyclotron maser—An historical survey," *IEEE Trans. Microwave Theory Tech.*, vol. MTT-25, pp. 522-527, 1977.
4. G. N. Rapoport, A. K. Nematik, and V. A. Zhurakhovskiy, "Interaction between helical electron beams and strong electromagnetic cavity-fields at cyclotron frequency harmonics," *Radio Eng. Electron. Phys.*, vol. 12, pp. 587-595, 1967.
5. G. S. Nusinovich and R. E. Erm, *Elektron Tekh.*, Ser. 1, *Elektron. SVCh*, No. 2, 55 (1972).
6. V. L. Bratman, M. A. Moiseev, M. I. Petelin, and R. E. Erm, "Theory of Gyrotrons with a Non-Fixed Structure of the High-Frequency Field," *Radiophys. Quantum Electron.* 16, 474-480 (1973).
7. S. V. Kolosov and A. A. Kurayev, "Comparative analysis of the interaction at the first and second harmonics of the cyclotron frequency in gyroresonance devices," *Radio Eng. Electron. Phys.*, vol. 19, no. 10, pp. 65-73, 1974.
8. A. A. Kurayev, F. G. Schevchenko, and V. P. Shestakovich, "Efficiently optimized output cavity profiles that provide a higher margin of gyrokystron stability," *Radio Eng. Electron. Phys.*, vol. 19, no. 5, pp. 96-103, 1974.
9. D. V. Kisel', G. S. Korablev, V. G. Navel'yev, M. I. Petelin, and S. E. Tsimring, "An experimental study of a gyrotron, operating at the second harmonic of the cyclotron frequency, with optimized distribution of the high frequency field," *Radio Eng. Electron. Phys.*, vol. 19, pp. 95-100, Apr. 1974.



10. A. V. Gaponov, A. L. Gol'denberg, D. P. Grigor'ev, T. B. Pankratova, M. I. Petelin and V. A. Flyagin, "Experimental Investigation of Centimeter Band Gyrotrons," *Radiophysics and Quantum Electron.* **18**, No. 2, 204-211 (1975).
11. S. N. Vlasov, G. M. Zhislin, I. M. Orlova, M. I. Petelin and G. G. Rogacheva, "Irregular Waveguides as Open Resonators," *Radiophysics and Quantum Electron.* **12**, No. 8, 972-978 (1969).
12. P. Sprangle and R. Smith, "The Nonlinear Theory of Efficiency Enhancement in the Electron Cyclotron Maser," Naval Research Laboratory Memo Report no. 3983 (to be published).
13. M. Read and R. Lucey, "Study on the Initial Development of High Power Millimeter Wave Sonics," Naval Research Laboratory Memo Report (unpublished).
14. K. R. Chu "Theory of Electron Cyclotron Maser Interaction in a Cavity at the Harmonic Frequencies," *Phys. of Fluids* **21**, 2354-2364 (1978).
15. P. Sprangle and A. T. Drobot, "The linear and self-consistent nonlinear theory of the electron cyclotron maser instability," *IEEE Trans. Microwave Theory Tech.*, vol. MTT-25, pp. 528-544, 1977.
16. K. R. Chu and A. T. Drobot, "Theory and Single Wave Simulation of the Gyrotron Travelling Wave Amplifier Operating at Cyclotron Harmonics," Naval Research Laboratory Memo Report No. 3788 (to be published).

17. K. R. Chu, A. T. Drobot, H. H. Sze, and P. Sprangle, "Analytical Scaling of Efficiency for the Gyrotron Travelling Wave Amplifier," Naval Research Laboratory Memo Report No. 3892 (to be published).
18. J. A. Seftor, A. T. Drobot, and K. R. Chu, "An Investigation of a Magnetron Injection Gun Suitable for Use in Cyclotron Resonance Masers," IEEE Trans. ED (in press).
19. H. R. Jory and R. S. Simons, private communication.



Table I. Optimum efficiency data for  $\alpha = 1.5$  and tapered magnetic field.

Data No.	1	2	3	4	5	6
Mode	$TE_{011}$	$TE_{011}$	$TE_{021}$	$TE_{031}$	$TE_{021}$	$TE_{031}$
$\bar{L}$	5	8	5	5	8	8
$\bar{r}_0$	0.48	0.48	0.26	0.18	0.26	0.18
$\bar{\omega}$	3.88	3.85	7.04	10.19	7.03	10.18
$\bar{B}_1$	3.69	3.85	7.17	10.76	7.47	11.07
$\Delta \bar{B}$	0.85	0.57	0.85	0.61	0.34	0.27
$\bar{E}_{\infty}$	0.22	0.15	0.24	0.25	0.16	0.12
$QP_n^{th} (MW)$	69	54	109	500	687	$\infty$
$QP_n^{opt} (MW)$	210	126	194	195	126	85
$QP_n (MW)$	83	62	100	109	70	40
$\eta^{opt} (\%)$	39.5	48.9	51.6	55.7	55.4	46.9
$N_c$	10.7	17.4	20.0	29.2	32.1	47.2

Table II. Optimum efficiency data for  $\alpha = 1.5$  and constant magnetic field.

Data No.	7	8	9	10	11	12
Mode	$TE_{011}$	$TE_{011}$	$TE_{021}$	$TE_{031}$	$TE_{021}$	$TE_{031}$
$\bar{L}$	5	8	5	5	8	8
$\bar{r}_0$	0.48	0.48	0.26	0.18	0.26	0.18
$\bar{\omega}$	3.88	3.85	7.04	10.19	7.03	10.18
$\bar{B}_0$	4.08	4.16	7.60	11.13	7.66	11.22
$\bar{E}_{\infty}$	0.20	0.13	0.18	0.15	0.10	0.08
$QP_n^{th} (MW)$	95	41	100	172	746	$\infty$
$QP_n^{opt} (MW)$	241	127	159	113	85	68
$QP_n (MW)$	68	43	55	40	29	18
$\eta^{opt} (\%)$	28.2	33.5	34.9	34.5	33.7	26.1
$N_c$	10.7	17.4	20.0	29.2	32.1	47.2

Table III. Optimum efficiency data for  $\alpha = 2$  and tapered magnetic field.

Data No.	13	14	15	16	17
Mode	$TE_{011}$	$TE_{011}$	$TE_{021}$	$TE_{031}$	$TE_{021}$
$\bar{L}$	5	8	5	5	8
$\bar{r}_0$	0.48	0.48	0.26	0.18	0.26
$\bar{\omega}$	3.88	3.85	7.04	10.19	7.03
$\bar{B}_1$	3.83	3.96	7.34	10.93	7.58
$\Delta \bar{B}$	0.59	0.37	0.49	0.34	0.21
$\bar{E}_{\infty}$	0.19	0.14	0.22	0.18	0.11
$QP_h^{th} (MW)$	45	80	400	7580	$\infty$
$QP_h^{opt} (MW)$	109	81	126	96	62
$QP_u (MW)$	62	54	82	56	34
$\eta^{opt} (\%)$	57.2	67.1	66.6	58.5	54.2
$N_c$	13.4	21.5	24.7	36.5	40.1

Table IV. Optimum efficiency data for  $\alpha = 2$  and constant magnetic field.

Data No.	18	19	20	21	22
Mode	$TE_{011}$	$TE_{011}$	$TE_{021}$	$TE_{031}$	$TE_{021}$
$\bar{L}$	5	8	5	5	8
$\bar{r}_0$	0.48	0.48	0.26	0.18	0.26
$\bar{\omega}$	3.88	3.85	7.04	10.19	7.03
$\bar{B}_0$	4.13	4.14	7.61	11.22	7.70
$\bar{E}_{\infty}$	0.15	0.10	0.15	0.14	0.08
$QP_h^{th} (MW)$	50	85	250	$\infty$	$\infty$
$QP_h^{opt} (MW)$	104	66	97	100	59
$QP_u (MW)$	40	27	39	34	18
$\eta^{opt} (\%)$	38.5	41.2	40.2	34.1	29.7
$N_c$	13.4	21.5	24.7	36.5	40.1



Table V. Optimum efficiency data for  $\alpha = 2.5$  and tapered magnetic field

Data No.	23	24	25	26	27	28
Mode	$TE_{011}$	$TE_{011}$	$TE_{021}$	$TE_{011}$	$TE_{021}$	$TE_{021}$
$\bar{L}$	4	6	4	8	5	6
$\bar{r}_a$	0.48	0.48	0.26	0.48	0.26	0.26
$\bar{\omega}$	3.91	3.87	7.06	3.85	7.04	7.04
$\bar{B}_1$	3.84	3.93	7.28	3.98	7.37	7.47
$\Delta\bar{B}$	0.61	0.44	0.61	0.30	0.45	0.30
$\bar{E}_{a_{01}}$	0.20	0.16	0.26	0.14	0.22	0.16
$QP_k^{th}$ (MW)	33	49	191	102	199	204
$QP_k^{opt}$ (MW)	82	72	123	69	108	74
$QP_w$ (MW)	55	53	94	54	84	53
$\eta^{opt}$ (%)	67.0	73.5	76.5	77.8	77.5	72.2
$N_c$	12.9	19.5	23.9	26.2	30.1	36.2

Table VI. Optimum efficiency data for  $\alpha = 2.5$  and constant magnetic field.

Data No.	28	30	31	32	33	34
Mode	$TE_{011}$	$TE_{011}$	$TE_{021}$	$TE_{011}$	$TE_{021}$	$TE_{021}$
$\bar{L}$	4	6	4	8	5	6
$\bar{r}_a$	0.48	0.48	0.26	0.48	0.26	0.26
$\bar{\omega}$	3.91	3.87	7.06	3.85	7.04	7.04
$\bar{B}_a$	4.12	4.15	7.63	4.18	7.68	7.71
$\bar{E}_{a_{01}}$	0.17	0.11	0.16	0.07	0.11	0.09
$QP_k^{th}$ (MW)	58	50	102	45	133	336
$QP_k^{opt}$ (MW)	97	56	83	32	54	49
$QP_w$ (MW)	40	25	36	13	21	17
$\eta^{opt}$ (%)	41.2	44.4	43.1	41.9	39.0	34.7
$N_c$	12.9	19.5	23.9	26.2	30.1	36.2

Table VII. Design parameters of a 35 GHz gyrotron oscillator based on data No. 14 in Table III.

Mode	$TE_{011}$
beam voltage	70 kV
beam current	2.31 Amp
$v_{10}/v_{00}$	2.0
cavity radius $r_w$	0.526 cm
cavity length $L$	4.208 cm
beam guiding center position $r_0$	0.252 cm
$B_1$	12.84 kG
$\Delta B$	1.20 kG
efficiency $\eta$	67.1 %
$Q$	500
threshold beam power $P_b^{th}$	160.0 kW
optimum beam power $P_b^{op}$	162.0 kW
output wave power $P_w$	108.7 kW



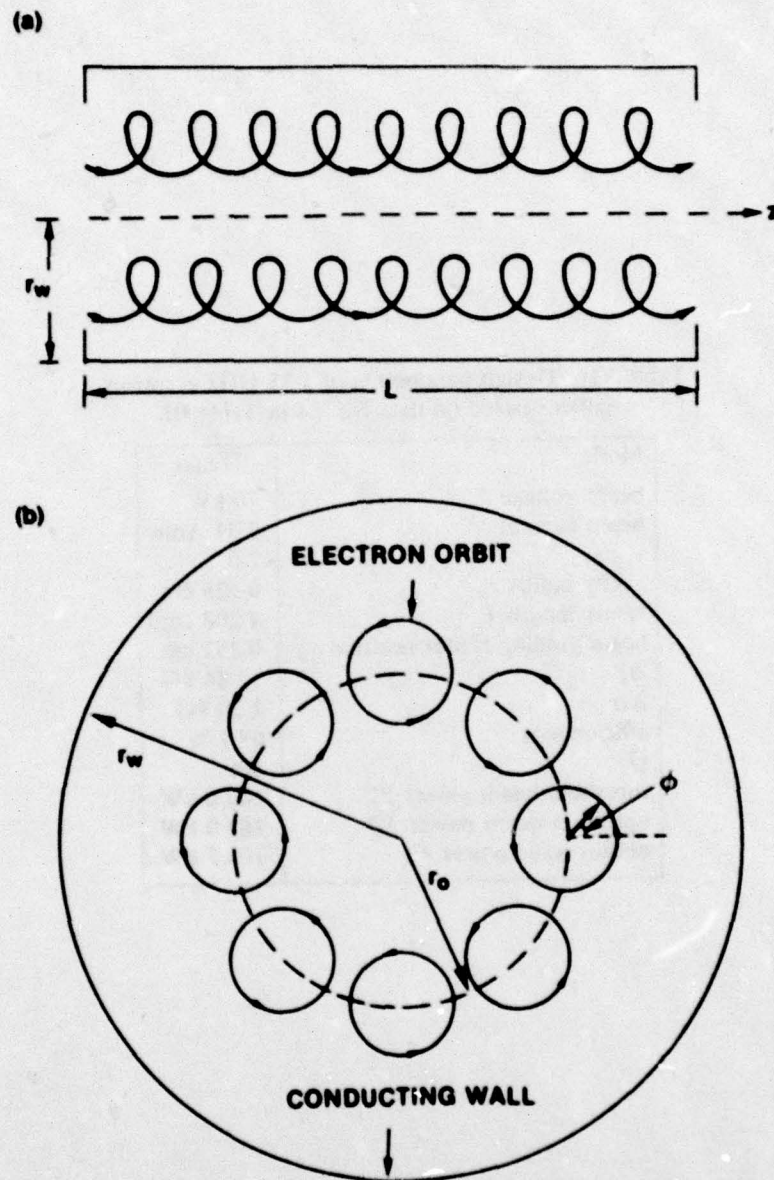


Fig. 1 — Side view (a) and end view (b) of the single cavity gyrotron oscillator.

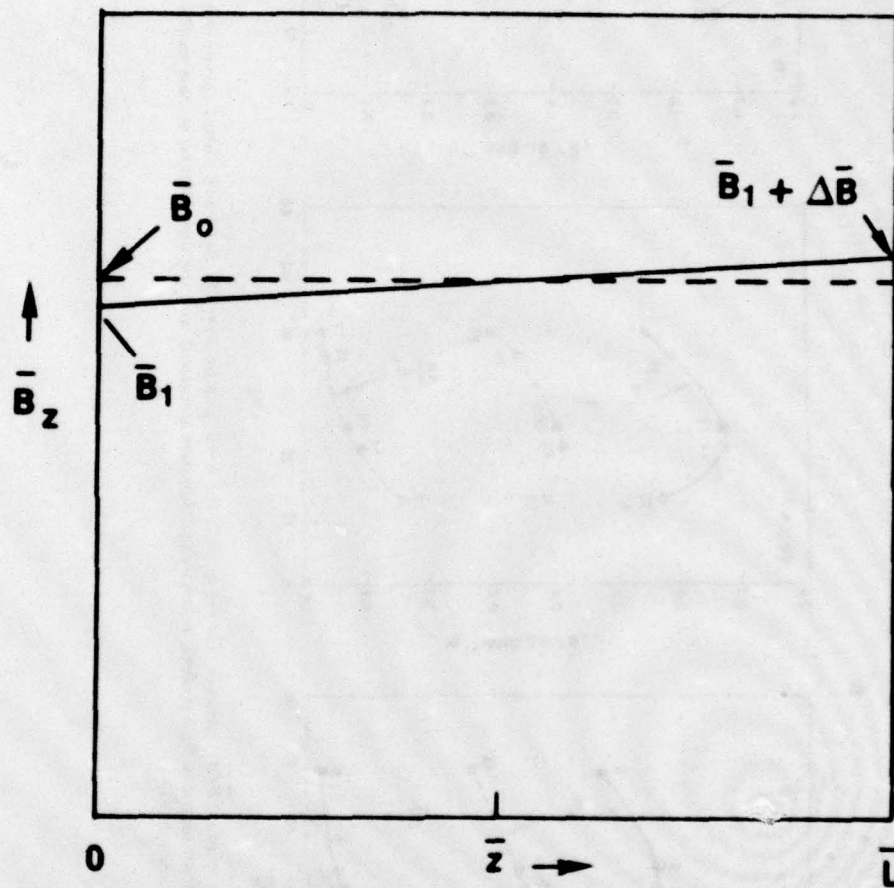


Fig. 2 = Typical profile of the tapered magnetic field (solid line). For comparison,  $B_z$  profile of the constant magnetic field is also plotted in dashed line.



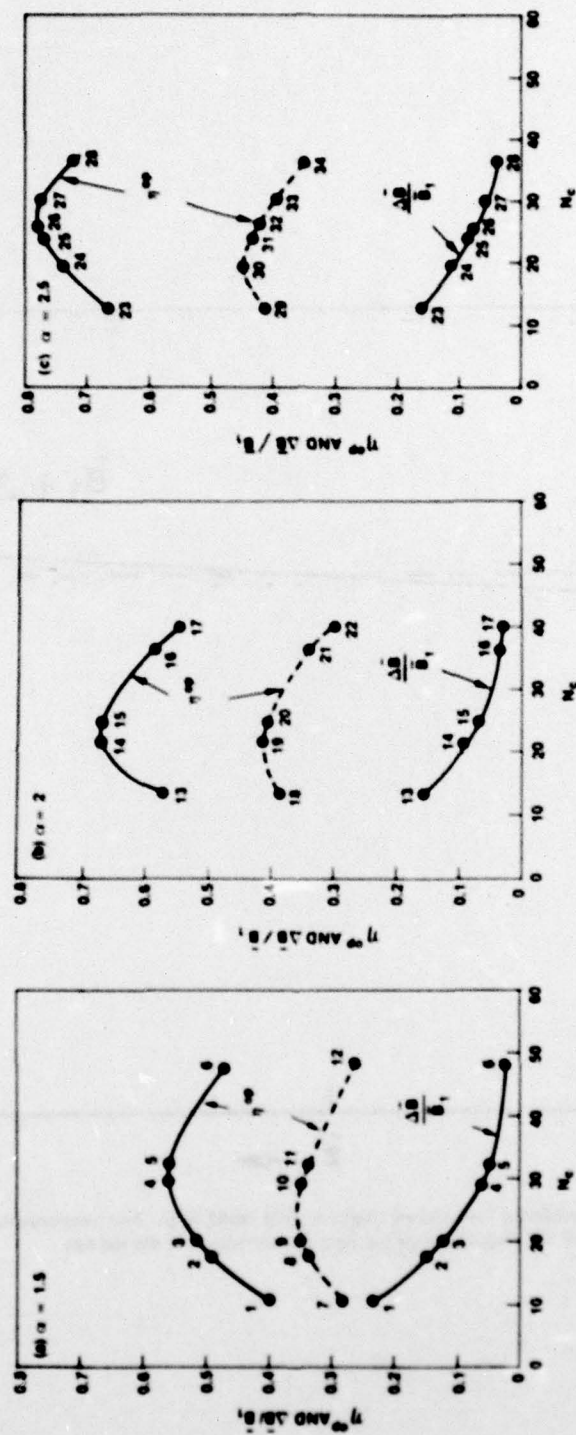


Fig. 3 —  $\eta$  and  $\Delta B/B_1$  versus  $N_c$  for (a)  $\alpha = 1.5$ , (b)  $\alpha = 2$ , and (c)  $\alpha = 2.5$ . Solid and dashed curves refer to tapered and constant magnetic field profiles, respectively. Numbers associated with the dots refer to the data numbers shown in Table I through VI.

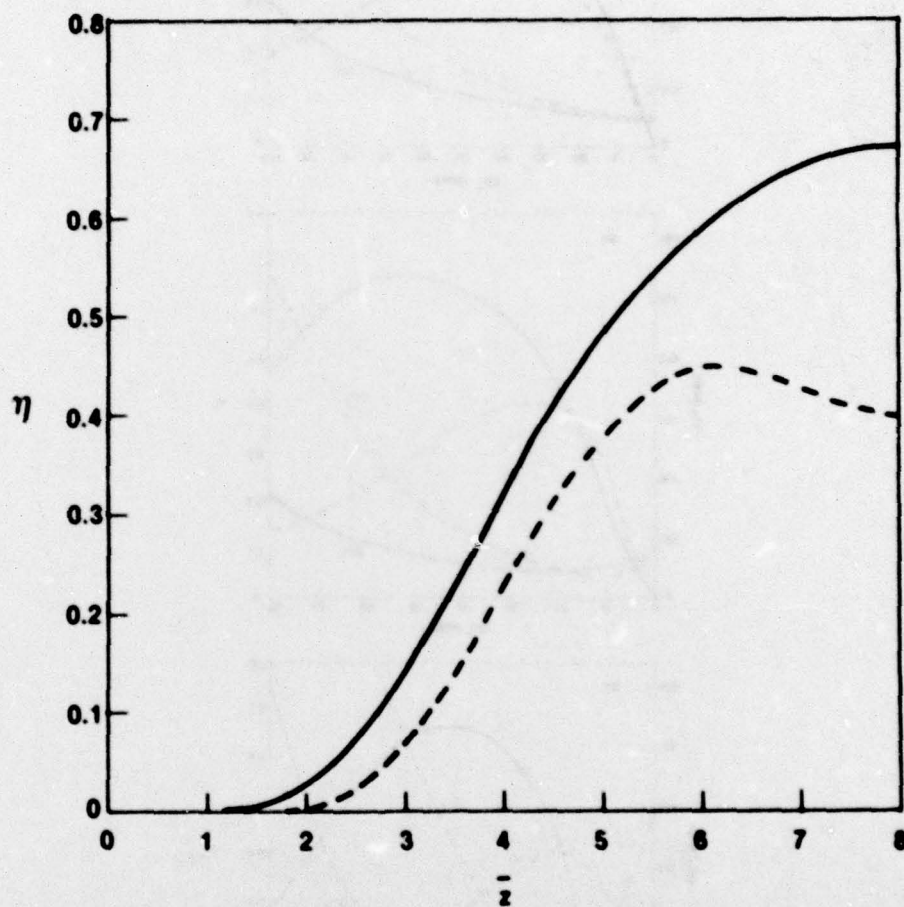


Fig. 4 —  $\eta$  versus  $\bar{z}$  for the  $TE_{011}$  mode,  $L=8$ , and  $\alpha=2$ . Solid and dashed curves refer to the tapered and constant magnetic field profiles, respectively.



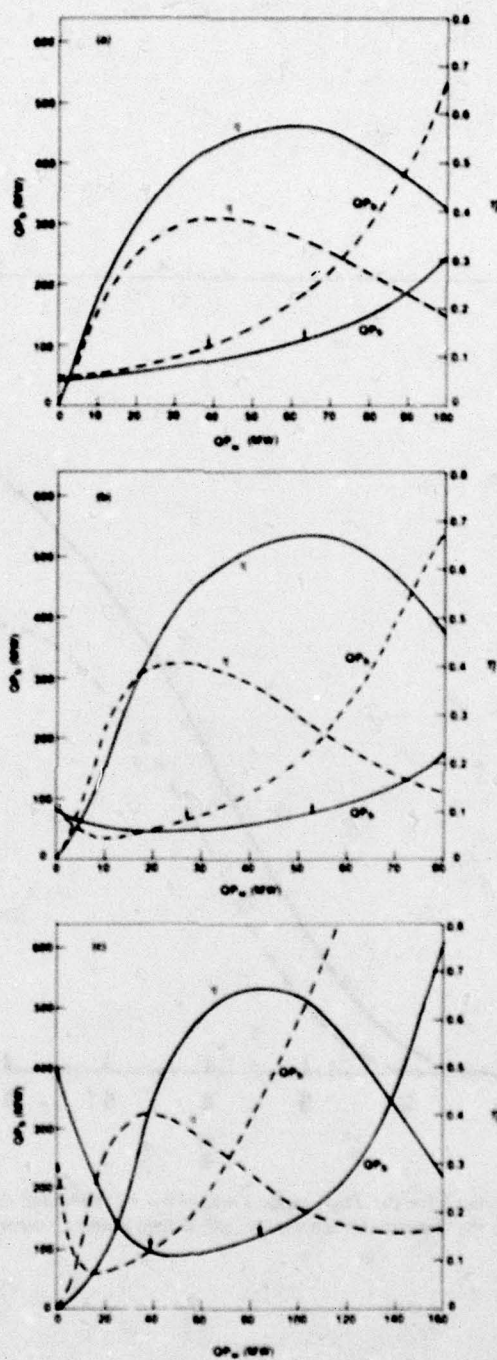


Fig. 5 -  $QP_s$  and  $\eta$  versus  $QP_u$  for  $\alpha=2$ . Solid and dashed curves refer to the tapered and constant magnetic field profiles, respectively.  $QP_s$  at  $QP_u=0$  gives the threshold beam power  $P_b^{th}$ .  $QP_s$  at the peak of  $\eta$  (marked by an arrow) gives the optimum beam power  $P_b^{op}$ . (a)  $TE_{011}$  mode,  $L=5$ ,  $N_t=13.4$ , (b)  $TE_{011}$  mode,  $L=8$ ,  $N_t=21.5$ , and (c)  $TE_{021}$  mode,  $L=5$ ,  $N_t=24.7$ .